Design optimization of medium specific speed Francis turbines with unshrouded runners

IOP Conf. Series: Earth and Environmental Science **240** (2019) 022060 doi:10.1088/1755-1315/240/2/022060

Design optimization of medium specific speed Francis turbines with unshrouded runners

W Takahashi [1], M Shinji [1], Z H Liu [1], K Miyagawa [2], and Y Hayashi [3]

[1] Department of Applied Mechanics, Waseda University, Tokyo, 1698555, Japan
[2] Department of Applied Mechanics and Aerospace Engineering, Waseda University, Tokyo, 1698555, Japan
[3] Research & Development Dept., Chigasaki Research Institute, Kanagawa, 2530041, Japan

E-mail: w-takahashi@fuji.waseda.jp

Abstract. In present, many undeveloped locations of small hydropower generation exist in Japan. To promote the use of small hydropower generation it is required to reduce costs and increase efficiency. Unshrouded runners are proposed to simplify the manufacturing process and also to reduce the manufacturing costs. In this paper, the computation results of optimized unshrouded runners are presented. This research was conducted to minimize the shroud tip leakage loss, which is the main loss of unshrouded runners. In the author's laboratory, medium specific speed (160 [m-kW]) Francis turbines was developed. For this 160 [m-kW] Francis turbines, investigation of internal flow and loss mechanism were done by computation. Using this loss mechanism which was revealed by rothalpy, the design of the same specific speed Francis turbines with unshrouded runners was optimized. For the new runners, shroud tip clearance and the pressure distribution of vane surfaces was changed. Due to this, shroud tip leakage flow has weakened. In the simulation of whole domain, 2.45% of improvement was confirmed on the design point.

1. Introduction

In present, global warming is regarded as a significant problem. Due to this, utilizing renewable sources of energy attracts attention. One of the most popular kind of these renewable energies is hydropower generation. Hydropower does not emit greenhouse gases and oxides which are the main cause of environmental problems. In these days, small and medium hydro turbine is focused on. However, there are some disadvantages, such as difficult to manufacture by casting, generates small amount of energy. In order to promote small hydropower generation, cost reduction and high efficiency is demanded. To achieve this, Francis turbines with unshrouded runners were proposed [1][2]. This simplifies the manufacturing process and reduce the manufacturing costs of the turbines.

In this paper, design of a medium specific speed Francis turbine with unshrouded runner was optimized. To design new hydro turbine, the accuracy of computation was confirmed through comparison with experiments of the conventional hydro turbine [3]. Then the loss mechanism of conventional hydro turbine was investigated [4]. It was found that leakage at the shroud tip is the main cause of loss in runners.

Computation was used to predict the internal flow in the design process. For the Runner Vane (RV), the shroud tip clearance and pressure distribution of vane surfaces was changed to improve the leakage

loss. For the complete hydro turbine, performance prediction was performed by computation. Improvement on the efficiency can be observed compared to conventional Francis turbines.

2. Details of Experiment

Figure 1 shows the overview of conventional model turbine test rig. Water start flowing from the overflow tank into the hydro turbine. Then it flows into the vacuum tank, and goes to the underground storage tank. The specification of the model turbine is shown in table 1.

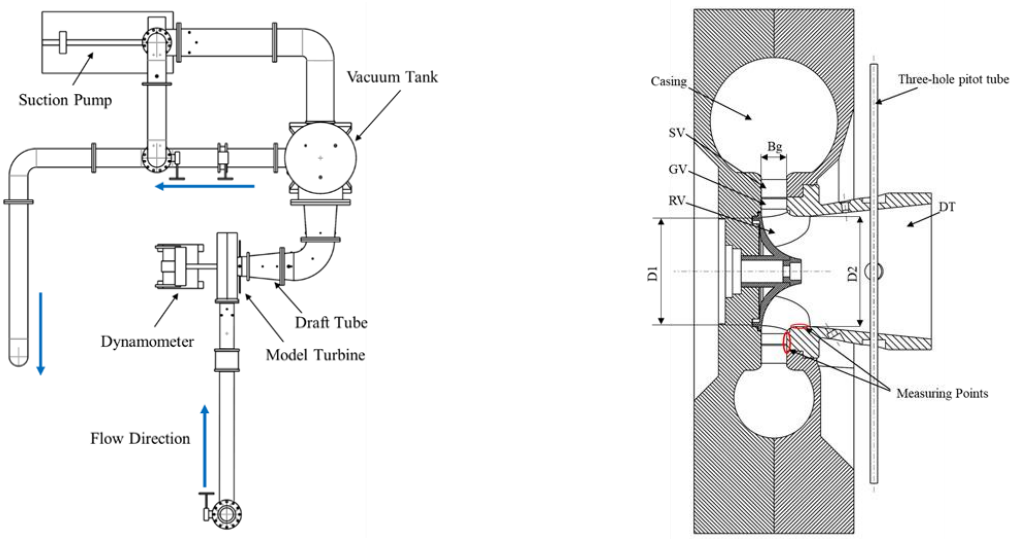

(a) Overview of model turbine test rig. **(b)** Cross section of model turbine.

Figure 1. Model turbine test rig.

Table 1. Specification of the conventional model turbine.

Items	Values	Units
Specific speed N_s	161.7	m-kW
Design point flow rate Q	0.07255	m^3/s
Design point rotation speed N	1500	rpm
Effective head H_e	14.68	m
Power P	9.60	kW
D_1	0.1578	m
D_2	0.1579	m
B_g	0.039	m
Number of SV* Z_s	20	-
Number of GV** Z_g	20	-
Number of RV Z_r	18	-

* Stay Vane
** Guide Vane

In table 1, the specific speed is defined as

$$N_s = NP^{1/2}/H_e^{5/4} \quad (1)$$

For the performance test, the Guide Vane Opening (GVO) was changed from 30% to 110% in increments of 10%. In each GVO, the rotation speed coefficient N_{11} was changed from 52 to 72 in increments of 5. The rotation speed coefficient (N_{11}), and the flow rate coefficient (Q_{11}) are defined as

$$N_{11} = ND_1/H_e^{1/2} \quad (2)$$

$$Q_{11} = Q/(D_1^2 H_e^{1/2}) \quad (3)$$

To investigate the internal flow of double circular cascade consisting of SV and GV, multipoint pressure sensor device (DSA) was used. The measurement holes are shown in figure 2. By using DSA, the static pressure was measured.

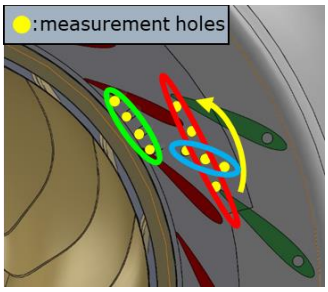

Figure 2. Measurement holes.

3. Computational Setup

The internal flow computation was performed by using Reynolds-Averaged Navier-Stokes equation (RANS) with the commercial code ANSYS CFX 17.2. For the turbulence model, Shear Stress Transport (SST k-ω) was used. When investigating inflow of turbines, SST k-ω is able to obtain good agreement with the experiment [5]. The computational domain includes 5 components: Casing, Stay Vanes, Guide Vanes, Runner Vanes, and Draft tube (DT) as shown in figure 3. For the new hydro turbine, the vane number of SV, GV, and RV are same as the conventional hydro turbine. The number of elements, the boundary treatment between stationary and rotor components, and the boundary condition are shown in table 2, 3, and 4, respectively. The mesh was tetrahedral or hexahedral.

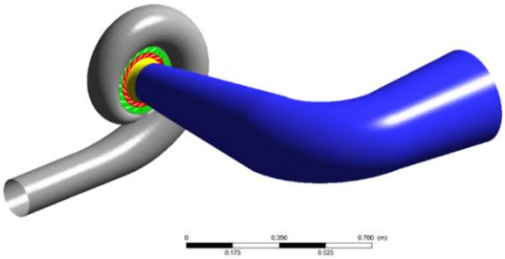

(a) View of full computational domain.
(gray: Casing, green: SV, red: GV, yellow: RV, blue: DT)

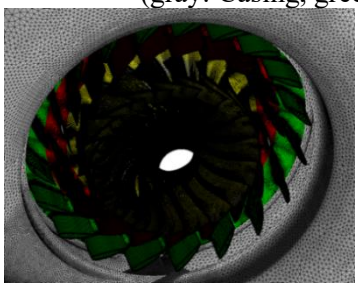

(b) Meshes of cascades.

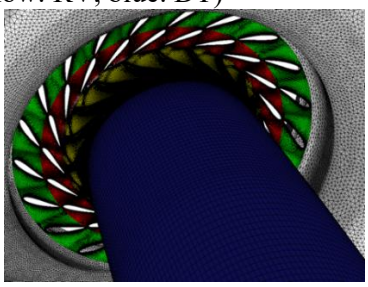

(c) Meshes of cascades with DT.

Figure 3. Computational domain.

Table 2. Mesh information.

		Conventional	New
Number of Elements	**Casing**	3,675,000	3,078,089
	SV	3,820,000	4,096,000
	GV	4,054,400	4,653,000
	RV	13,979,520	19,378,440
	DT	2,226,774	2,042,033
	Total	27,755,694	33,247,562

Table 3. Boundary condition.

Casing inlet	Total Pressure
DT outlet	Static Pressure

Table 4. Boundary treatment of stationary and rotor components.

GV-RV	Mixing-Plane (Stage Average Velocity)
RV-DT	Frozen Rotor

4. Results and Discussions

4.1 *Results of Conventional Hydro Turbine*

In this section, the performance test results and the computation results of conventional hydro turbine were compared, as shown in figure 4. In figure 4 (b), Hydraulic efficiency (η_h) and Q_{11} are normalized by the value of best efficiency point (B.E.P), respectively. η_h is defined as

$$\eta_h = \tau\omega/(\rho g Q H_e) \quad (4)$$

Where τ and ω are torque and angular velocity, respectively.

Also, results of internal flow measurement using DSA are shown in figure 5. The horizontal axis shows the angle from the beginning of the casing and the vertical axis shows the normalized static pressure (C_{ps}) which is defined as

$$C_{ps} = P_s/(0.5\rho V_1^2) \quad (5)$$

Where ρ, and V_1 are density and velocity of casing inlet, respectively. It is seen in figures 4 and 5 that experimental and computation results are in good agreement. From these results, it was confirmed that computation by CFD is suitable for designing hydro turbine.

For the cavitation test, it was unable to lower the Thoma cavitation number than 0.08. For this reason, it was not able to determine the point of degradation in performance.

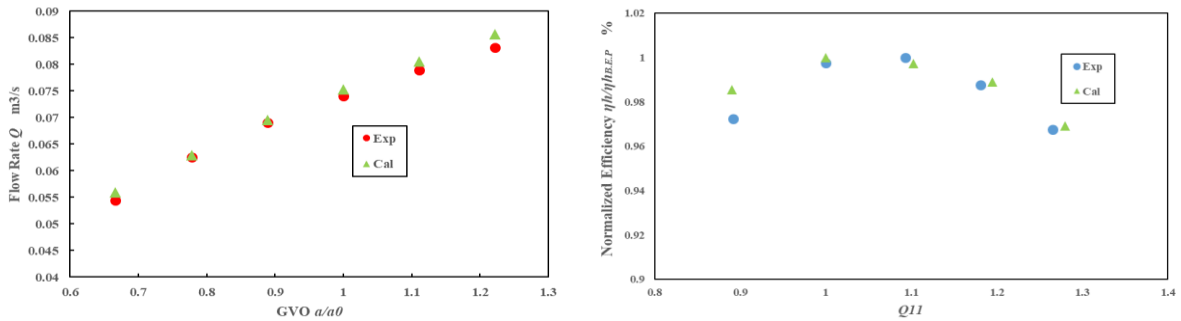

(a) Flow rate of each GVO. **(b)** Efficiency curve.

Figure 4. Comparison of performance test and computation.

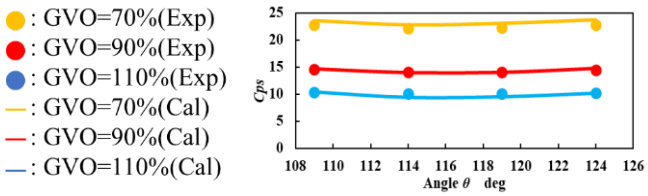

(a) SV-GV circumferential distribution.

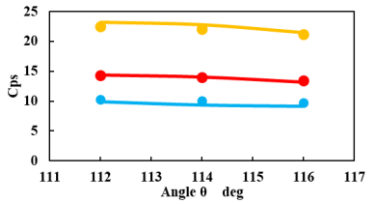

(b) GV streamwise distribution.

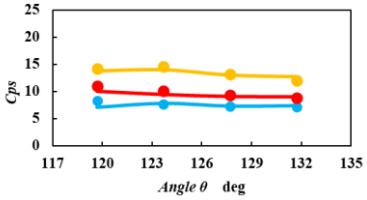

(c) GV outlet circumferential distribution.

Figure 5. Static distribution of double circular cascade.

4.2 *Loss Mechanism of Conventional RV*

To optimize RV, the loss mechanism of conventional RV was investigated. Rothalpy definition was adopted to estimate the loss of RV. To estimate loss in the rotor, rothalpy is more suitable rather than using total pressure or enthalpy [6]. Rothalpy (I) is defined as

$$\mathrm{I} = \mathrm{h} + 0.5(W^2 - U^2) \tag{6}$$

Where h, W, and U are enthalpy, relative velocity, and rotation velocity, respectively. The normalized rothalpy loss (C_r) contour is shown in figure 6. Cr is defined as

$$C_r = (I_{R1} - I)/(gH_e) \tag{7}$$

Where I_{R1} and g are rothalpy of RV inlet and gravitational acceleration, respectively. To investigate the rothalpy loss, surfaces were made in near leading edge (LE), mid-chord, and near trailing edge (TE), which is shown in figure 6. From figure 7, it can be inferred that the rothalpy loss gets larger as it goes to the TE.

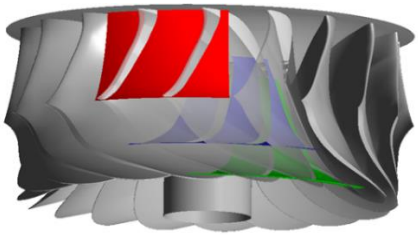

Figure 6. Surface setup on conventional RV.
(Red:Near LE, Blue:Mid-chord, Green:Near TE)

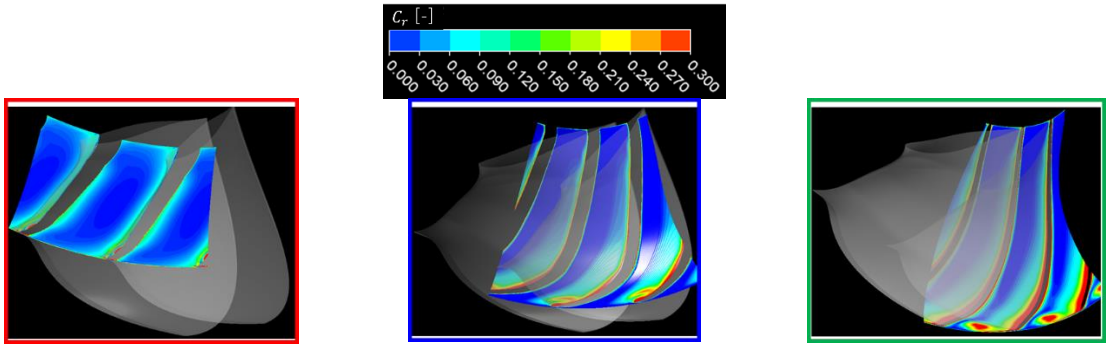

(a) Near LE. **(b)** Mid-chord. **(c)** Near TE.

Figure 7. Normalized rothalpy loss in conventional RV (GVO=90%).

The enlarged view of figure 7 is shown in figure 8. Also, to investigate the loss mechanism of figure 7, contour of kinetic energy coefficient of secondary flow (C_{ke}) was used. Which is shown in figure 9. C_{ke} is defined as

$$C_{ke} = V_{sec}/V_{ave} \quad (8)$$

Where V_{sec} and V_{ave} are secondary flow velocity and averaged bulk velocity, respectively. From these figures, it was known that there were mainly 2 kinds of flow. One is the secondary flow from crown to shroud, and the other is the leakage flow at the shroud tip. In the figure 9 (a), near the LE, the secondary flow from crown was stronger than the leakage flow. This induced the vortex in counter-clockwise and loss region in figure 8 (a). In the figure 9 (b), at the mid-chord, the deflection of secondary flow is small. Due to this, the vortex in counter- clockwise began to collapse. In the figure 9 (c), near TE, leakage flow got much stronger which deflected the secondary flow and induced the vortex in clockwise and loss region. Because of these results, it was considered that leakage flow was the main cause of loss at RV.

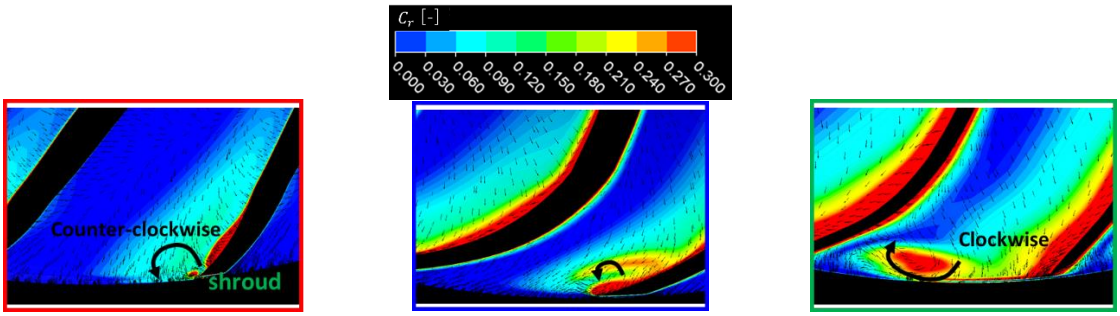

(a) Near LE. **(b)** Mid-chord. **(c)** Near TE.

Figure 8. Enlared view of normalized rothalpy loss (GVO=90%).

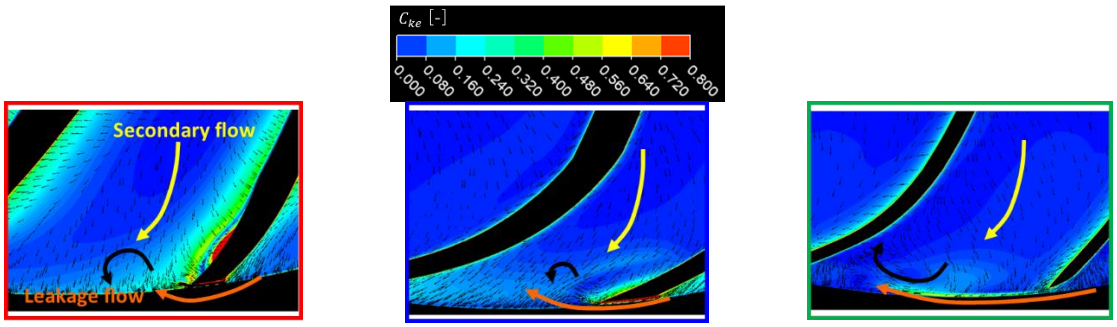

(a) Near LE. **(b)** Mid-chord. **(c)** Near TE.

Figure 9. Kinetic energy coefficient of secondary flow in conventional RV (GVO=90%).

5. Optimizations of RV

5.1 *Improvement of RV Upstream*

To rectify the RV inflow, SV and GV were optimized. The number of SV and GV was not changed, but the profile and the relative position were changed. These are shown in figure 10. Also, this shows the normalized total pressure loss (C_{pt}) of mid span. C_{pt} is defined as

$$C_{pt} = (Pt_{C1} - Pt)/(\rho g H_e) \quad (9)$$

Where Pt_{C1} is total pressure of casing inlet. It was seen from figure 10 that the SV wake flow was extending until the downstream of GV in the conventional type. Contrary to this, the extension of SV wake flow decreased in the new type. In figure 10, it was confirmed that, significant difference was seen in GVO=90%. The wake from SV has decreased, and the losses at GV outlet has decreased. This was also confirmed from figure 11. This shows the comparison of GV loss distribution in each GVO. GVO of each operating point is 70%, 80%, 90% (design point), 100%, and 110% from the left, respectively.

From figure 11, it was said that the GV loss has decreased not only on design point, but also on other operating points.

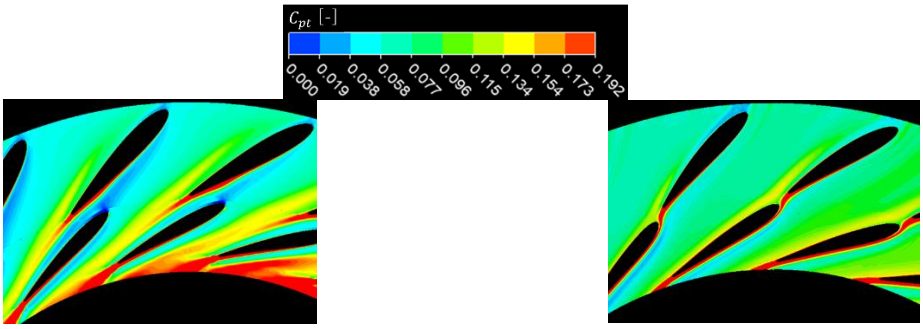

(a) Conventional. **(b)** New.

Figure 10. Comparison normalized total pressure loss in SV and GV (GVO=90%).

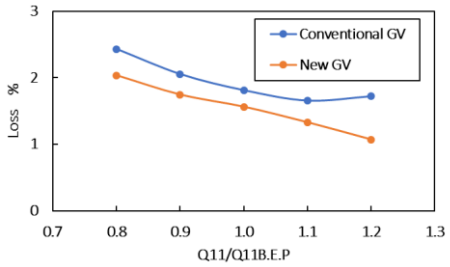

Figure 11. Comparison of GV loss distribution in each GVO.

5.2 *Improvement of RV*

To reduce the shroud tip leakage loss, shroud tip clearance and the form of TE were changed. First, for the shroud tip clearance, it was changed from 0.3 mm to 0.2 mm. Due to this change, the leakage flow ratio (C_q) was decreased from 2.93% to 1.34%. C_q is defined as

$$C_q = (Q_i - Q_l)/Q_i \quad (10)$$

Where Q_i and Q_l are flow rate of casing inlet and leakage flow rate, respectively.

For the pressure distribution of vane surfaces, the conventional RV had high load near the LE as shown in figure 12. This type of load distribution will be called front-loaded for this paper. Contrary to this, RV which has high load near TE will be called aft-loaded. In figure 12, vertical axis shows the normalized static pressure (C_p) which is defined as

$$C_p = Ps/(\rho g H_e) \quad (11)$$

However, front-loaded generates stronger vortex, and higher secondary loss than the aft-loaded [7]. Due to this, the new RV was changed to aft-loaded by changing the vane angle. Figure 13 shows the vane angle distribution.

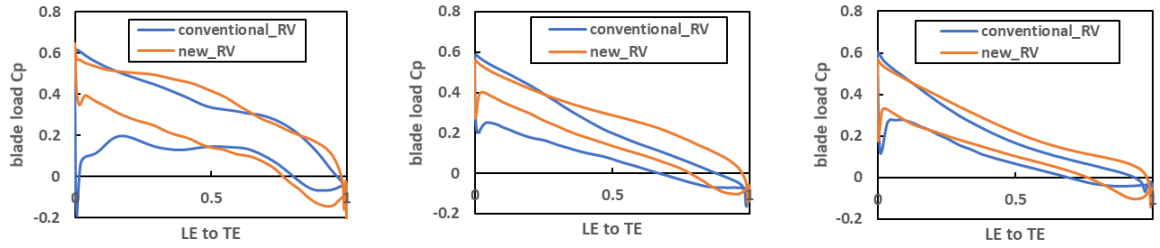

(a) shroud. **(b)** mid. **(c)** crown.

Figure 12. Comparison of pressure distribution on vane surface (GVO=90%).

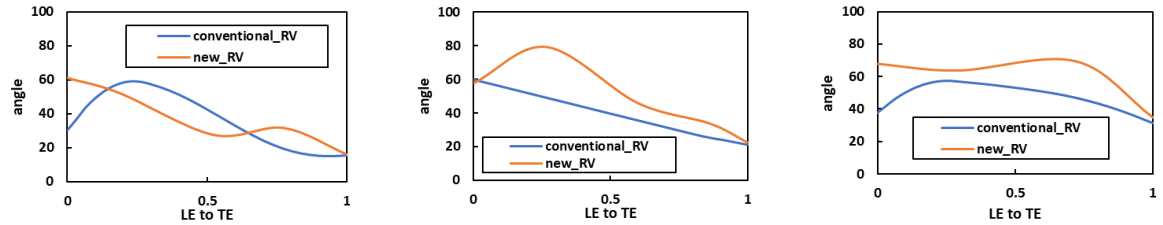

(a) shroud. **(b)** mid. **(c)** crown.

Figure 13. Comparison of vane angle distribution.

By changing to aft-loaded, the shape of RV was changed from figure 14 (a) to figure 14 (b). As shown in figure 14, the TE was drastically changed. Figure 15 shows the vectors of leakage and secondary flow on the cross section near TE. As in figure 15, the TE of conventional RV is warped to suction side. This leads the leakage flow keeping very fast velocity. On the other hand, for the new RV, TE was warped to pressure side. In this form, near around shroud on the suction side became a shape like a diffuser, and the leakage flow was decelerated. Because of this the leakage flow was weakened than the conventional RV. This was confirmed in figure 17. Figure 16 shows the measurement surface, and figure 17 shows the C_r contour.

(a) Conventional RV. **(b)** New RV.

Figure 14. RV view from shroud.

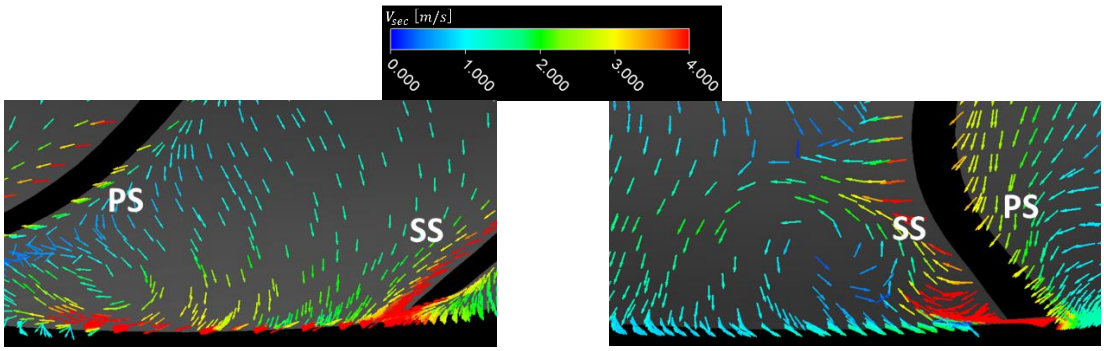

(a) Conventional RV. **(b)** New RV.

Figure 15. Secondary flow vector (GVO=90%).

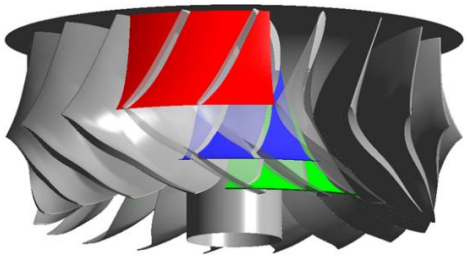

Figure 16. Surface setup on new RV.
(Red:Near LE, Blue:Mid-chord, Green:Near TE)

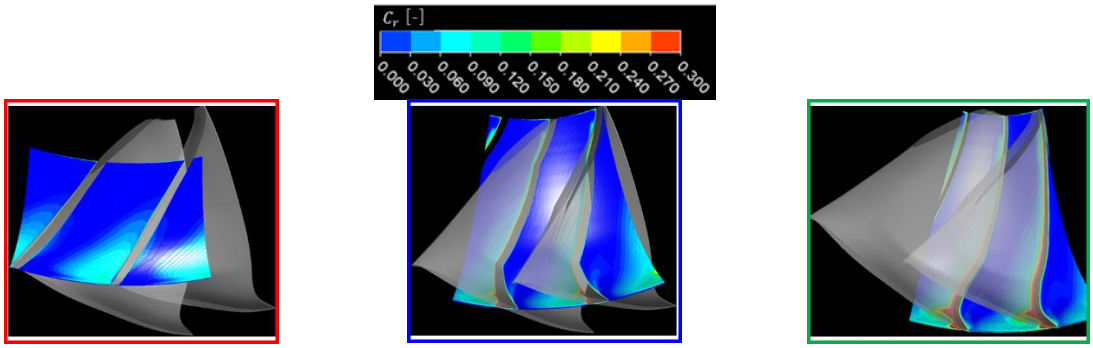

(a) Near LE. **(b)** Mid-chord. **(c)** Near TE.

Figure 17. Normalized rothalpy loss in new RV (GVO=90%).

The enlarged view of figure 17 is shown in figure 18. Also, to investigate the loss mechanism of figure 18, contour of C_{ke} was used. Which is shown in figure 19. Near the LE, the secondary flow from crown was stronger than the leakage flow. This phenomenon is same as the conventional RV. This induced the vortex in counter-clockwise and loss region. However, the different phenomenon was seen from the mid chord. In the conventional RV at mid chord and near the TE, the leakage flow was stronger than the secondary flow. But in the new RV, the leakage flow did not become stronger, which was confirmed in Figure 19 (b) and (c). Because of this, leakage flow was not strong enough to deflect the secondary flow. Therefore, the loss has been decreased.

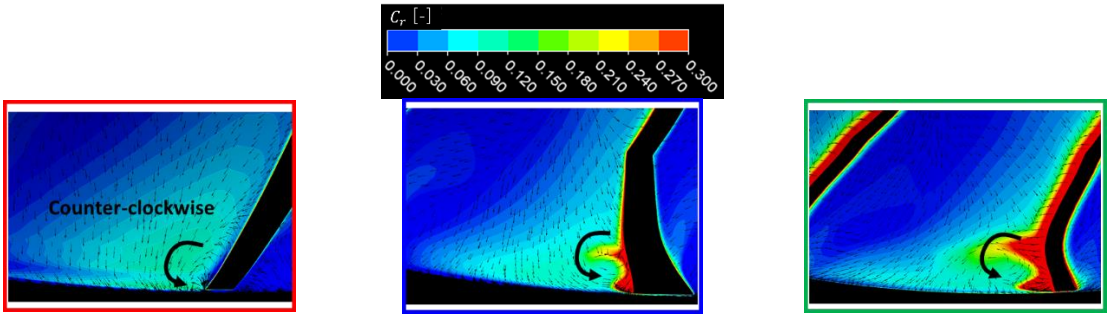

(a) Near LE. **(b)** Mid-chord. **(c)** Near TE.

Figure 18. Enlared view of normalized rothalpy loss (GVO=90%).

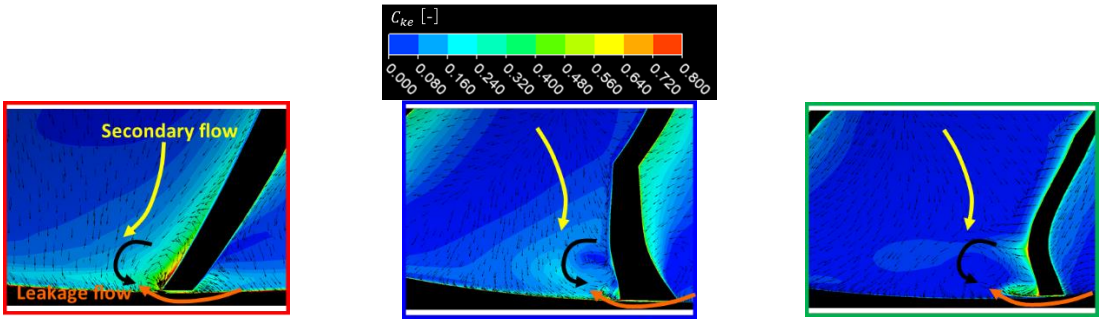

(a) Near LE. **(b)** Mid-chord. **(c)** Near TE.

Figure 19. Kinetic energy coefficient of secondary flow in new RV (GVO=90%).

6. Computation Results

The computation results of complete hydro turbine are shown in figure 20. η_h and Q_{11} are normalized by the value of best efficiency point (B.E.P), respectively. GVO of each operating point is 70%, 80%, 90% (design point), 100%, and 110% from the left, respectively. Therefore, it can be known from figure 20 that the conventional hydro turbine's B.E.P was not on design point. Contrary to this, new hydro turbine had the B.E.P on design point, and 2.45% of best efficiency was improved. Figure 21 shows the loss distribution in each operating point. The GVO of each operating point is same as figure 20.

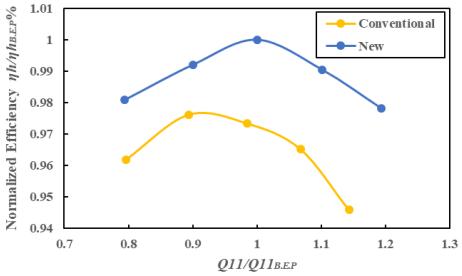

Figure 20. Efficiency curve ($N_{11} = 62$).

As in figure 21, loss of stationary parts improved 0.45% and RV improved 2.0% at GVO=90%. Moreover, RV improved 1.5% and 2.0% at GVO=70% and 110%, respectively. Therefore, to figure out the factor of improvement at these operating points, RV were investigated. Same method was used to investigate. Figure 22 and figure 23 show the comparison of C_r contour of GVO=70% and GVO=110%, respectively. From these figures, it was confirmed that the loss region has decreased. Same phenomenon in GVO=90% happened in these 2 operating points. Due to this, it is said that the RV loss has decreased not only on the design point but, also on off-design points.

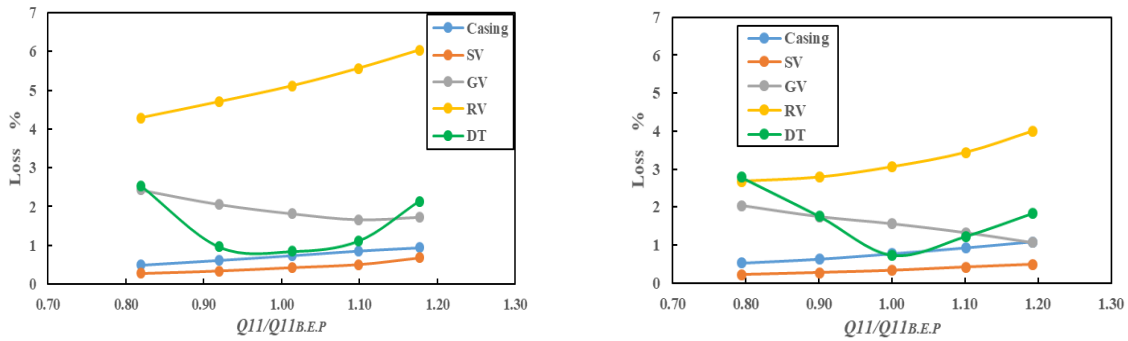

(a) Conventional hydro turbine. **(b)** New hydro turbine.

Figure 21. Loss distribution in each operating point.

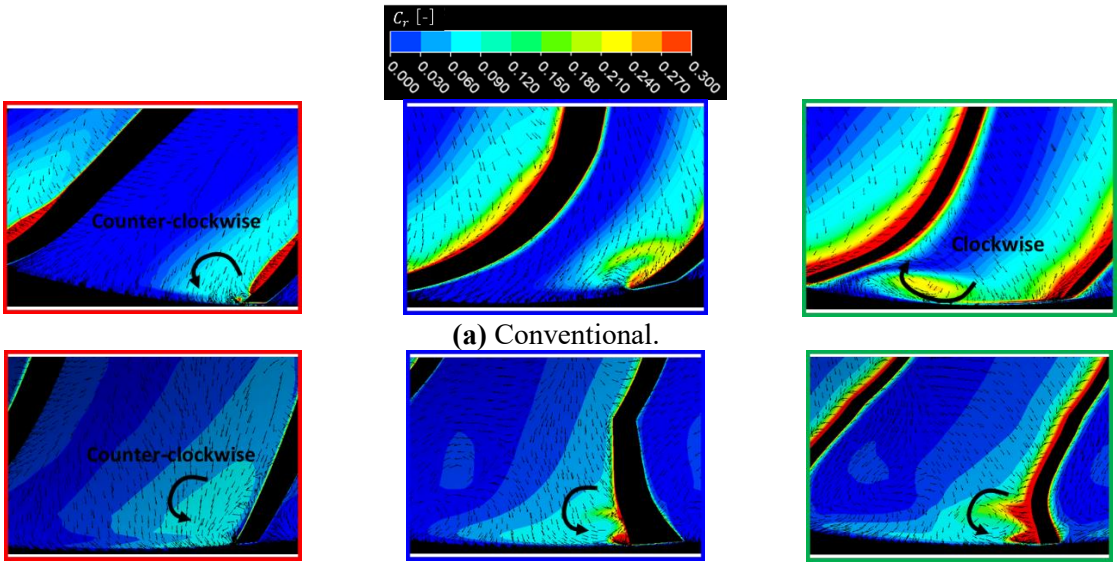

(a) Conventional.

(b) New.

Figure 22. Comparison of normalized rothalpy loss in RV (GVO=70%).

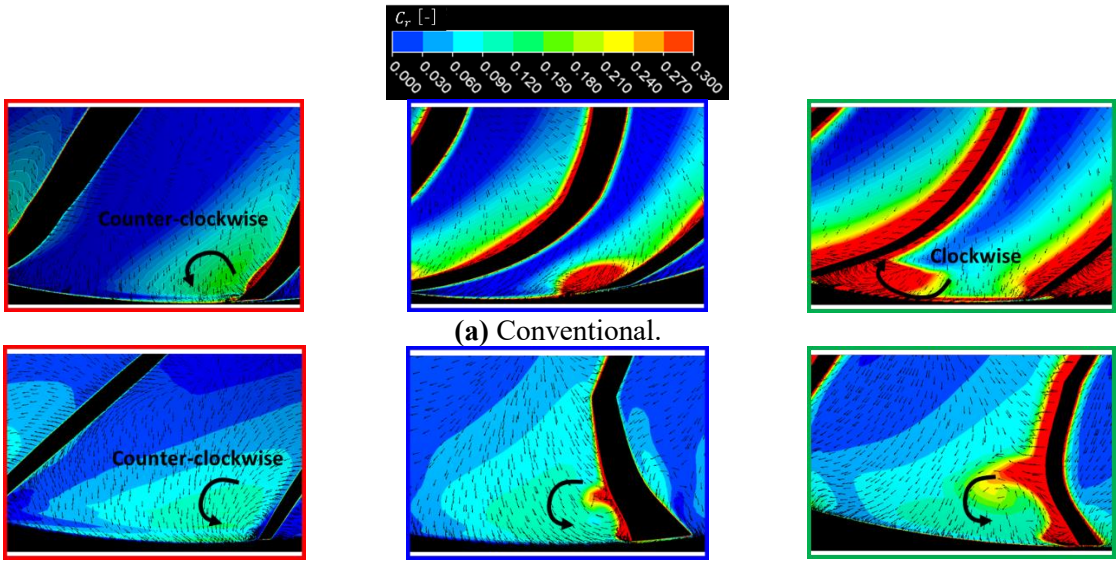

(a) Conventional.

(b) New.

Figure 23. Comparison of normalized rothalpy loss in RV (GVO=110%).

7. Conclusions

The good agreement of experimental and computation results was confirmed. By using the computation, a new medium specific speed Francis turbine with unshrouded RV was optimized. The conclusions were as follows.

(1) Computation by CFD is suitable for designing hydro turbine.
(2) The shroud tip leakage loss is the main loss in the unshrouded runners.
(3) Shroud tip leakage flow was decelerated by changing the pressure distribution on vane surfaces.
(4) 2.45% of improvement in the design point was confirmed for the new hydro turbine.

8. Acknowledgments
The authors would like to thank the Waseda Research Institute for Science and Engineering (WISE) for providing support to the presented research, in context of the project: 'High performance and high reliability research for hydraulic turbomachinery systems'

References
[1] Y Nakamura, R Shima, H Komatsu, S Shiratori and K Miyagawa 2015 Development of Shroudless Francis Turbine by *ASME/JSME/KSME 2015 Joint Fluids Engineering Conference*, American Society of Mechanical Engineers, pp. V01AT02A006-V01AT02A006
[2] Y Nakamura, H Komatsu, S Shiratori, R Shima, S Saito and K Miyagawa 2015 Development of high-efficiency and low-cost shroudless turbine for small hydropower generation plant by *The Proceedings of the International Conference on Power Engineering (ICOPE) 2015.12*, The Japan Society of Mechanical Engineers, pp. _ICOPE-15
[3] Z H Liu, M Shinji, and K Miyagawa 2017 Internal flow and loss mechanisms of specific speed 160 m-kW shroudless hydro turbine by *AWG-IAHR*
[4] K Miyagawa, K Yasuda, Y Iwasaki 2000 Study on internal flow and new design technology for a Francis turbine runner by *20th IAHR Symposium on Hydraulic Machinery and Sysytems*, pp. 1-10.
[5] S K Krishnababu, P J Newton, W N Dawes, G D Lock, H P Hodson, J Hannis, and C Whitney 2008 Aerothermal Investigations of Tip Leakage Flow in Axial Flow Turbines—Part I: Effect of Tip Geometry and Tip Clearance Gap by *ASME. J. Turbomach*, pp. 2008;131(1):011006-011006-14. doi:10.1115/1.2950068
[6] F A Lyman 1992 On the Conservation of Rothalpy in Turbomachines by *ASME. Turbo Expo: Power for Land, Sea, and Air, Volume 1: Turbomachinery*(), pp. V001T01A078. doi:10.1115/92-GT-217
[7] A P Weiss and L Fottner 1993 The Influence of Load Distribution on Secondary Flow in Straight Turbine Cascades by *ASME. Turbo Expo: Power for Land, Sea, and Air, Volume 1: Aircraft Engine; Marine; Turbomachinery; Microturbines and Small Turbomachinery* (), pp. V001T03A027. doi:10.1115/93-GT-086